HHS Public Access

Author manuscript

Science. Author manuscript; available in PMC 2017 July 25.

Published in final edited form as:

Science. 2016 July 08; 353(6295): 158–162. doi:10.1126/science.aaf4292.

Phototactic guidance of a tissue-engineered soft-robotic ray

Sung-Jin Park[1], **Mattia Gazzola**[2,†], **Kyung Soo Park**[3,4,‡], **Shirley Park**[5,§], **Valentina Di Santo**[6], **Erin L. Blevins**[6,‖], **Johan U. Lind**[1], **Patrick H. Campbell**[1], **Stephanie Dauth**[1], **Andrew Capulli**[1], **Francesco S. Pasqualini**[1], **Seungkuk Ahn**[1], **Alexander Cho**[1], **Hongyan Yuan**[1,¶], **Ben M. Maoz**[1], **Ragu Vijaykumar**[5], **Jeong-Woo Choi**[3,4], **Karl Deisseroth**[5,7], **George V. Lauder**[6], **L. Mahadevan**[2,8], and **Kevin Kit Parker**[1,4,*]

[1]Disease Biophysics Group, Wyss Institute for Biologically Inspired Engineering, John A. Paulson School of Engineering and Applied Sciences, Harvard University, Cambridge, MA 02138, USA

[2]John A. Paulson School of Engineering and Applied Sciences, Harvard University, Cambridge, MA 02138, USA

[3]Department of Chemical and Biomolecular Engineering, Sogang University, Seoul 121-742, Korea

[4]Sogang-Harvard Research Center for Disease Biophysics, Sogang University, Seoul 121-742, Korea

[5]Department of Bioengineering, Stanford University, Stanford, CA 94305, USA

[6]Museum of Comparative Zoology, Harvard University, Cambridge, MA 02138, USA

[7]Department of Psychiatry and Behavioral Sciences and the Howard Hughes Medical Institute, Stanford University, Stanford, CA 94305, USA

[8]Department of Organismic and Evolutionary Biology, Department of Physics, Wyss Institute for Biologically Inspired Engineering, Kavli Institute for Nanobio Science and Technology, Harvard University, Cambridge, MA 02138S

Abstract

Inspired by the relatively simple morphological blueprint provided by batoid fish such as stingrays and skates, we create a biohybrid system that enables an artificial animal, a tissue-engineered ray,

[*]Correspondence to: K.K.P. 29 Oxford Street, Pierce Hall Cambridge, MA 02130. kkparker@seas.harvard.edu. Phone: 617-495-2850, 617-835-5920. Fax: 617-496-1793.

[†]Current Address: Department of Mechanical Science and Engineering, University of Illinois at Urbana-Champaign, Urbana, IL 61801, USA

[‡]Current Address: Department of Biomedical Engineering, University of Michigan, Ann Arbor, MI 48109, USA.

[§]Current Address: Cardiovascular Medicine, Stanford University Medical Center, Stanford, CA 94305, USA.

[‖]Current Address: The Winsor School, Boston, MA 02215, USA

[¶]Current Address: Department of Mechanical, Industrial and Systems Engineering, University of Rhode Island, Kingston, RI 02881, USA

Supplementary Materials:

Materials and Methods
Supplementary Text
Figures S1–S15
Tables S1
Movies S1–S20
References (33–44)

to swim and phototactically follow a light cue. By patterning dissociated rat cardiac myocytes on an elastomeric body enclosing a microfabricated gold skeleton, we replicated fish morphology at one-tenth scale and captured basic fin deflection patterns of batoid fish. Optogenetics allows for phototactic guidance, steering and turning maneuvers. Optical stimulation induced sequential muscle activation via serpentine patterned muscle circuits leading to coordinated undulatory swimming. The speed and direction of the ray was controlled by modulating light frequency and by independently eliciting right and left fins, allowing the biohybrid machine to maneuver through an obstacle course. (125/125 max)

Bioinspired design, as applied to robotics, aims at implementing naturally occurring features such as soft materials, morphologies, gaits, and control mechanisms in artificial settings to improve performance (1–4). For example, recent soft-robotics studies raised awareness on the importance of material properties (3, 4), shifting the focus from rigid elements to soft materials, while other investigations report successful mimicry of gaits or morphological features inspired by insects (5, 6), fish (7, 8), snake (9), salamanders (10) and cheetahs (11). While recent advances have the promise of bridging the performance gap with animals, the current soft-robotic actuators based on, for instance, electroactive polymers, shape memory alloys or pressurized fluids, are yet to mature to the point of replicating the high-resolution complex movements of biological muscles (3, 4).

In this context, biosensors and bioactuators (12) are intriguing alternatives, since they can intrinsically respond to a number of control inputs (such as electric fields and optical stimulation). Thanks to recent advances in genetic tools (13) and tissue engineering (12), these responses can be altered and tuned across a wide range of time and length scales. Some pioneering studies have exploited these technologies for self-propulsion, developing miniaturized walking machines (14–16), and flagellar (17) or jellyfish inspired (18) swimming devices. These biohybrid systems operate at high energy efficiency and harvest power from energy dense, locally available nutrients, although at present they require specialized environments (physiological solutions) that may limit their applicability. Moreover and most importantly, these biohybrid locomotors lack of the reflexive control (9, 19) necessary to enable adaptive maneuvering and thus of the ability to respond to spatiotemporally varying external stimuli.

Here, we design, build and test a tissue-engineered analog of a batoid fish such as stingrays and skates. By combining soft materials and tissue engineering with optogenetics, we created an integrated sensory-motor system that allowed for coordinated undulating fin movement and phototactically controlled locomotion, that is guided via light stimuli. We drew from fish morphology, neuromuscular dynamics and gait control to implement a living, bio-hybrid system that leads to robust and reproducible locomotion and turning maneuvers. Batoid fish are ideal biological models in robotics (8) because their nearly planar bauplan is characterized by a broad dorsoventral disk, with a flattened body and extended pectoral fins, that enhances stability against roll (20). They swim with high energy efficiency (21) by generating spanwise bending deformations and chordwise front-to-rear undulatory motion (20, 22) (Fig. 1A and movie S1) via the sequential activation of pectoral fin muscles. This undulatory gait allows slender aquatic animals to channel body movement into forward

motion by exchanging momentum with the fluid (7, 22), and is a convergent mode of aquatic propulsion (23). Moreover, batoids can employ these undulatory modes for fine maneuvering and turning by independently and asymmetrically actuating their pectoral fins (24). Inspired by the batoids, we reverse-engineered their musculoskeletal structure (Fig. 1B and fig. S1) via a four-layered architecture (Fig. 1C): a 3D elastomer (polydimethylsiloxane, PDMS) body cast via a titanium mold (fig. S2A and movie S2); a chemically neutral skeleton fabricated by thermal evaporation of gold through a custom designed shadow mask; a thin interstitial elastomer layer obtained by spin-coating; and finally a layer of aligned rat cardiomyocytes generated via microcontact printing of fibronectin (fig. S3) (25).

This design yielded a tissue-engineered ray with a single muscle layer capable of downward contraction (Fig. 1, C and D). Upward contraction would require a second layer of muscle that acts antagonistically to the upper layer. To minimize the complexity of our design, we instead used an asymmetrical stiff gold skeleton that stores elastic energy during the downstroke and rebounds during the subsequent relaxation phase. Inspired by histological analysis (fig. S1) as well as theoretical considerations (26), we channeled muscular work and elastic energy into forward motion by breaking fore-aft symmetry through a varying body rigidity along the anterior-posterior axis. This was achieved via a thicker body, and a denser and radially further reaching skeleton pattern in the front (Fig. 1, C and D, Fig. 2A, and fig. S2A). Likewise, along the proximal-distal axis, flexibility of the fins was enhanced by gradually reducing their thickness (fig. S2A). Finally, the PDMS mixture was adjusted (25) to provide body rigidity and fin flexibility while conserving overall neutral buoyancy (fig. S2).

The composite supporting structure described above was coupled to a tissue-engineered muscle layer which captured the salient musculoskeletal features of batoid fish (Fig. 2B). At the mesoscale (50 μm – 5 mm), batoids myofibers are tightly bundled and are aligned in the radial direction parallel to the rays of the skeleton (Fig. 2B). At the microscale (1 – 10 μm), the Z-lines of the sarcomeres (the cell force generating units – Fig. 2C) present strong nematic alignment perpendicular to individual myofibers so as to focus contraction forces. Following this layout, the muscles and sarcomeres of the tissue-engineered ray were designed to orient radially from the body and parallel to the gold skeleton rays (Fig. 2B and fig. S4), while the Z-lines of the sarcomeres were engineered to be perpendicular to the skeleton rays through microscale patterning of fibronectin (Fig. 2C and fig. S4).

Finally, to mimic the sensory-somatic nervous system that controls the sequential activation of fin muscle in the batoid fish, we recast the neuro-control problem into a design one. A possible solution is given by serpentine patterned muscle circuits that physically determine the propagation of muscle contraction in space and time (Fig. 1D and Fig. 2, D and E), leading to hardwired coordination that could be triggered with external stimuli. This design was implemented by overlaying onto anisotropic tissue, a layer of cardiomyocytes that were electrically coupled with gap junctions (fig. S4H). These myocytes were engineered to respond to optical stimuli (Fig. 1, D) by expressing a light-sensitive ion channel (channelrhodopsin-2, ChR2) (27). Thus, a point light stimulus directed at the front of the ray triggers the propagation of an action potential that is spatially and temporally modulated by the gap junctions between muscle cells without the need for neural coupling and

coordination (Fig. 2, D and E). The expression of ChR2 was obtained via lentiviral transduction mediated by the truncated cardiac troponin T promoter cTnT (25, 28) (fig. S5). This approach led to 88% transduction rate of cardiomyocytes and maximized the sensitivity to blue light at powers of ~10 mW (fig. S5).

Optical stimulation of the circuits initiated sequential activation waves that propagated along the anterior-posterior axis as revealed by calcium imaging (25) for three different circuit designs (Fig. 2D, fig. S6, and movie S3 and S4). Dense serpentine patterns enhanced activation localization, whereas rarefied ones increased propagation speed (fig. S7 and S8). To allow for maneuverability, we ensured that each pectoral fin could be independently actuated by pacing left and right optical stimuli at different frequencies (fig. S6 and movie S5). Among the various designs considered, the circuit of choice was characterized by the intermediate serpentine pattern density (Fig. 2E). This circuit represented the best tradeoff between overlap with batoids' operating range and contraction time reproducibility (low standard error), to minimize desynchronization and undesired turning (Fig. 2E). The final overall design of our ray consists of ~200,000 live cardiomyocytes, in an elastomeric body of 16.3 mm length and 10.18 ± 0.43 mg mass.

When immersed in a 37°C Tyrode's physiological salt solution containing glucose as energy reservoir, and upon optical stimulation, the fabricated ray propelled by producing forward thrust via the undulatory motion of its fins (Fig. 3 and movie S6). Video-tracking analysis (25) showed that during each swimming cycle, as the calcium signal propagated (fig. S9), the anterior region bent downward, while the posterior one lifted upward (Fig. 3, A and B), conferring a small downward orientation (−10°) to the ray's longitudinal axis (fig. S9). Both regions reached their maximum displacement around ~200 ms (Fig. 3B) when their motion gradually inverted until ~340 ms (Fig. 3, C and D). At this point, the calcium wave had traveled ~70% of the ray body and approached the flexible tail region (Fig. 3E and fig. S9). This signal caused a rapid, strong downward contraction of the rear of the body, a quick upward recoil of the head region (presumably mediated by the stiff skeleton - Fig. 3), a 30° upward reorientation of the longitudinal axis (fig. S9), and a spike in forward swimming speed (Fig. 3E). After 340 ms, the calcium wave vanishes and the ray relaxes (Fig. 3E and fig. S9), gliding until its forward momentum dissipates.

A periodical optical stimulation leads to a rhythmically sustained forward displacement (Fig. 3F). To test the benefits of spatiotemporally modulated undulatory locomotion relative to pulsatile locomotion (typical jellyfish), we stimulated our design of choice via global electrical fields (25). The latter, unlike optical point stimulation, induces a global, synchronized contraction of the entire muscle layer, leading to jet-like propulsion (movie S7). While pulsatile actuation also produced forward motion, undulatory gaits were found to be twice as fast at 1.5 Hz pacing (Fig. 3G).

We compared the kinematics (Fig. 3, H and I) and hydrodynamics (Fig. 3, J to M) of bio-inspired and live rays. Both rays exhibit asymmetric deformation patterns in which the deflection amplitude progressively increases in the radially outward and anterior-posterior directions. This similarity shows that our asymmetric composite structure compensates for the lack of the upper muscle layer (Fig. 3, B and D), leading to the coordinated undulatory

locomotion. Our design of choice was found to outperform a symmetric design (by 5.7 times, as measured by distance traveled per unit time) as well as asymmetric designs without gold skeleton (2.7×), with denser gold skeleton (8.2×), and with thinner (1.5×) and thicker fins (3.3×) (fig. S10 and movie S8 and S9). Particle image velocimetry (PIV) (25) images of the hydrodynamic footprint of the tissue-engineered ray (Fig. 3, A to D) show that body contractions generate vortices of alternating sign that are sequentially shed downstream in the wake (Fig. 3, A to D and movie S10), the hallmark of inertial undulatory swimming (29). Indeed, PIV of live skates (Fig. 3, K to M and S11) reveals a qualitatively similar alternation of positive and negative vortices, respectively generated in concave and convex regions of the body.

We emphasize here that our ray is a ten-fold scaled down version of a live skate and moves in a laminar flow regime, as opposed to batoid fish that operate in turbulent conditions. Thus, a direct performance comparison is not meaningful, but it is instructive to contextualize artificial and natural solutions in terms of a recent scaling framework (23, 30). All inertial undulatory swimmers hew to two scaling laws, $Re = Sw^{4/3}$ in the laminar regime and $Re = Sw$ in the turbulent regime, where the Swimming number $Sw = 2\pi fAL/\upsilon$, (L=the characteristic length of the swimmer, f=undulation frequency and A=amplitude, and υ=fluid viscosity) captures input kinematics, and the Reynolds number $Re = UL/\upsilon$ (with U=the forward speed) captures output speed. By fitting extant biological data (23), average swimming ‘rooflines’ were determined, thus providing an objective way to assess swimming performance. In this analysis, our tissue-engineered rays reached up to 63% of the Reynolds number of comparable natural solutions at the given Swimming number (Fig. 3J).

For gait control, we first determined a set of gait protocols for speed and direction control by modulating light frequency and by synchronously or asynchronously triggering the right and left serpentine circuits (fig. S11 and S12, movies S12 to S18). Synchronous pacing on both fins resulted in straight, forward displacement (fig. S11 and S12, movies S12 and S13), while stimulation frequency determined the swimming speed range (maximum at 1.5–2 Hz, minimum at 1 or 3 Hz – fig. S10E and movies S14 to S16). Asynchronous pacing instead resulted in directional turns (fig. S12, B, C, and F). In order to minimize the turning radius, we paired stimulation frequencies (1/1.5 Hz in movie S17, or 3/1.5 Hz in movie S18) to maximize the actuation difference between fins. Our ray turned in either clockwise and counter-clockwise directions by generating asymmetric undulating motion between left and right fins, as in batoid fishes (24).

Finally, we challenged the tissue-engineered ray to swim through an obstacle course. Using the above gait and turning protocols, we guided the ray along a curved path -by alternating forward motion and turning maneuvers, at an average speed of ~1.5 mm/s over a distance of ~250 mm, 15 times longer than its body length (Fig. 4 and movie S19). Furthermore, the ray was found able to maintain 80% of its initial speed for up to 6 consecutive days (fig. S13 and movie S20). Therefore, our ray outperformed existing locomotive biohybrid systems in terms of speed (3.2 mm/s in movie S16, 1.3× over jellyfish (18)), distance travelled (~250 mm, 35× over cantilever-like walkers (15)), and durability (6 days), demonstrating the potential of self-propelled, phototactically activated tissue-engineered robots.

With dissociated cells, naturally equipped with biosensors and bioactuators, as a programmable, actuating building material, we used optogenetics and tissue engineering to build an adaptive swimming animal. Our study is but a first step in engineering multi-level systems that link neurodynamics, mechanics and complex controllable gaits – coupling sensory information to motor coordination and movement that leads to behavior. This work paves the way for the development of autonomous and adaptive artificial creatures able to process multiple sensory inputs and produce complex behaviors in distributed systems and may represent a path toward soft-robotic “embodied cognition” (4, 31).

Supplementary Material

Refer to Web version on PubMed Central for supplementary material.

Acknowledgments

Data reported in the paper are included in the supplementary materials. We thank A. P. Nesmith, M. McKenna and A. Chandler for discussion on design, and K. Hudson and Margherita Gazzola for photography and illustrations. This work was funded by the Harvard Paulson School of Engineering and Applied Sciences, the Wyss Institute for Biologically Inspired Engineering, the National Center for Advancing Translational Sciences #UH3TR000522, Subcontract #312659 from Los Almos National Laboratory under prime DTRA contract #DE-AC52-06NA25396, the National Science Foundation (NSF) #EFRI-0938043, NSF MRSEC #DMR-1420570, Office of Naval Research MURI #N000141410533, the Swiss National Science Foundation, the MacArthur Foundation, the Radcliffe Institute, the National Research Foundation of Korea #2013K1A4A3055268, and the U.S. Army Research Laboratory and Office Contract #W911NF-12-2-0036. The views and conclusions contained in this document are those of the authors and should not be interpreted as representing official policies, expressed or implied, of the Army Research Office or Laboratory, the U.S. Government, or any other funding agencies. The U.S. Government is authorized to reproduce and distribute reprints for Government purposes notwithstanding any copyright notation hereon. Portions of this work were performed at the Center for Nanoscale Systems (NSF ECS-0335765), and at the Neurobiology Imaging Facility (NINDS P30 Core Center NS072030). Certain aspects of the paper are described in US patent 8,492,150 and US patent application 20150182679.

Full References

1. Pfeifer R, Lungarella M, Iida F. Self-organization, embodiment, and biologically inspired robotics. Science. 2007; 318:1088–1093. DOI: 10.1126/science.1145803 [PubMed: 18006736]
2. Haberland M, Kim S. On extracting design principles from biology: I. Method-General answers to high-level design questions for bioinspired robots. Bioinspir Biomim. 2015; 10:14.doi: 10.1088/1748-3190/10/1/016010
3. Kim S, Laschi C, Trimmer B. Soft robotics: a bioinspired evolution in robotics. Trends Biotechnol. 2013; 31:23–30. DOI: 10.1016/j.tibtech.2013.03.002
4. Rus D, Tolley MT. Design, fabrication and control of soft robots. Nature. 2015; 521:467–475. DOI: 10.1038/nature14543 [PubMed: 26017446]
5. Ma KY, Chirarattananon P, Fuller SB, Wood RJ. Controlled flight of a biologically inspired, insect-scale robot. Science. 2013; 340:603–607. DOI: 10.1126/science.1231806 [PubMed: 23641114]
6. Koh JS, Yang E, Jung GP, Jung SP, Son JH, Lee SI, Jablonski PG, Wood RJ, Kim HY, Cho KJ. Jumping on water: surface tension-dominated jumping of water striders and robotic insects. Science. 2015; 349:517–521. DOI: 10.1126/science.aab1637 [PubMed: 26228144]
7. Triantafyllou MS, Triantafyllou GS. An efficient swimming machine. Scientific American. 1995; 272:40–45. 48. DOI: 10.1038/scientificamerican0395-64
8. Moored KW, Fish FE, Kemp TH, Bart-Smith H. Batoid fishes: inspiration for the next generation of underwater robots. Mar Technol Soc J. 2011; 45:99–109. DOI: 10.4031/MTSJ.45.4.10
9. Astley HC, Gong C, Dai J, Travers M, Serrano MM, Vela PA, Choset H, Mendelson JR III, Hu DL, Goldman DI. Modulation of orthogonal body waves enables high maneuverability in sidewinding

locomotion. Proc Natl Acad Sci U S A. 2015; 112:6200–6205. DOI: 10.1073/pnas.1418965112 [PubMed: 25831489]

10. Ijspeert AJ, Crespi A, Ryczko D, Cabelguen JM. From swimming to walking with a salamander robot driven by a spinal cord model. Science. 2007; 315:1416–1420. DOI: 10.1126/science.1138353 [PubMed: 17347441]
11. Hyun DJ, Seok S, Lee J, Kim S. High speed trot-running: Implementation of a hierarchical controller using proprioceptive impedance control on the MIT Cheetah. Int J Robot Res. 2014; 33:1417–1445. DOI: 10.1177/0278364914532150
12. Chan V, Asada HH, Bashir R. Utilization and control of bioactuators across multiple length scales. Lab on a chip. 2014; 14:653–670. DOI: 10.1039/c3lc50989c [PubMed: 24345906]
13. Sander JD, Joung JK. CRISPR-Cas systems for editing, regulating and targeting genomes. Nature biotechnology. 2014; 32:347–355. DOI: 10.1038/nbt.2842
14. Feinberg AW, Feigel A, Shevkoplyas SS, Sheehy S, Whitesides GM, Parker KK. Muscular thin films for building actuators and powering devices. Science. 2007; 317:1366–1370. DOI: 10.1126/science.1146885 [PubMed: 17823347]
15. Chan V, Park K, Collens MB, Kong H, Saif TA, Bashir R. Development of Miniaturized Walking Biological Machines. Sci Rep. 2012; 2:8.doi: 10.1038/srep00857
16. Raman R, Cvetkovic C, Uzel SGM, Platt RJ, Sengupta P, Kamm RD, Bashir R. Optogenetic skeletal muscle-powered adaptive biological machines. Proc Natl Acad Sci U S A. 2016; 113:3497–3502. DOI: 10.1073/pnas.1516139113 [PubMed: 26976577]
17. Williams BJ, Anand SV, Rajagopalan J, Saif MTA. A self-propelled biohybrid swimmer at low Reynolds number. Nat Commun. 2014; 5:8.doi: 10.1038/ncomms4081
18. Nawroth JC, Lee H, Feinberg AW, Ripplinger CM, McCain ML, Grosberg A, Dabiri JO, Parker KK. A tissue-engineered jellyfish with biomimetic propulsion. Nature biotechnology. 2012; 30:792–797. DOI: 10.1038/nbt.2269
19. Braitenberg, V. Vehicles: Experiments in Synthetic Psychology. MIT Press; Cambridge, MA: 1986.
20. Rosenberger LJ, Westneat MW. Functional morphology of undulatory pectoral fin locomotion in the stingray Taeniura lymma (Chondrichthyes : Dasyatidae). J Exp Biol. 1999; 202:3523–3539. [PubMed: 10574730]
21. Di Santo V, Kenaley C. Skating by: low energetic costs of swimming in a batoid fish. J Exp Biol. 2016; 219doi: 10.1242/jeb.136358
22. Blevins EL, Lauder GV. Rajiform locomotion: three-dimensional kinematics of the pectoral fin surface during swimming in the freshwater stingray Potamotrygon orbignyi. J Exp Biol. 2012; 215:3231–3241. DOI: 10.1242/jeb.068981 [PubMed: 22693031]
23. Gazzola M, Argentina M, Mahadevan L. Scaling macroscopic aquatic locomotion. Nat Phys. 2014; 10:758–761. DOI: 10.1038/nphys3078
24. Parson JM, Fish FE, Nicastro AJ. Turning performance of batoids: Limitations of a rigid body. J Exp Mar Biol Ecol. 2011; 402:12–18. DOI: 10.1016/j.jembe.2011.03.010
25. Materials and methods are available as supplementary materials on Science Online.
26. Gazzola M, Argentina M, Mahadevan L. Gait and speed selection in slender inertial swimmers. Proc Natl Acad Sci U S A. 2015; 112:3874–3879. DOI: 10.1073/pnas.1419335112 [PubMed: 25770221]
27. Boyden ES, Zhang F, Bamberg E, Nagel G, Deisseroth K. Millisecond-timescale, genetically targeted optical control of neural activity. Nat Neurosci. 2005; 8:1263–1268. DOI: 10.1038/nn1525 [PubMed: 16116447]
28. Ma H, Sumbilla CM, Farrance IK, Klein MG, Inesi G. Cell-specific expression of SERCA, the exogenous Ca2+ transport ATPase, in cardiac myocytes. American journal of physiology Cell physiology. 2004; 286:C556–564. DOI: 10.1152/ajpcell.00328.2003 [PubMed: 14592812]
29. van Rees WM, Gazzola M, Koumoutsakos P. Optimal shapes for anguilliform swimmers at intermediate Reynolds numbers. J Fluid Mech. 2013; 722:12.doi: 10.1017/jfm.2013.157
30. Cotel AJ, Webb PW. Living in a turbulent world-a new conceptual framework for the interactions of fish and eddies. Integr Comp Biol. 2015; 55:662–672. DOI: 10.1093/icb/icv085 [PubMed: 26141867]

31. Pfeifer R, Marques H, Iida F. Soft robotics: the next generation of intelligent machines. Proceedings of the Twenty-Third International Joint Conference on Artificial Intelligence. 2013:5–11.
32. Muller UK, van Leeuwen JL. Swimming of larval zebrafish: ontogeny of body waves and implications for locomotory development. J Exp Biol. 2004; 207:853–868. DOI: 10.1242/jeb.00821 [PubMed: 14747416]
33. Agarwal A, Goss JA, Cho A, McCain ML, Parker KK. Microfluidic heart on a chip for higher throughput pharmacological studies. Lab on a chip. 2013; 13:3599–3608. DOI: 10.1039/c3lc50350j [PubMed: 23807141]
34. Pasqualini FS, Sheehy SP, Agarwal A, Aratyn-Schaus Y, Parker KK. Structural phenotyping of stem cell-derived cardiomyocytes. Stem cell reports. 2015; 4:340–347. DOI: 10.1016/j.stemcr.2015.01.020 [PubMed: 25733020]
35. Zhang F, Gradinaru V, Adamantidis AR, Durand R, Airan RD, de Lecea L, Deisseroth K. Optogenetic interrogation of neural circuits: technology for probing mammalian brain structures. Nat Protoc. 2010; 5:439–456. DOI: 10.1038/nprot.2009.226 [PubMed: 20203662]
36. Thielicke WS, Stamhuis EJ. PIVlab – Towards user-friendly, affordable and accurate digital particle image velocimetry in MATLAB. Journal of Open Research Software. 2014; 2:10.doi: 10.5334/jors.bl
37. Hedrick TL. Software techniques for two- and three-dimensional kinematic measurements of biological and biomimetic systems. Bioinspir Biomim. 2008; 3:034001.doi: 10.1088/1748-3182/3/3/034001 [PubMed: 18591738]
38. Standen EM, Lauder GV. Dorsal and anal fin function in bluegill sunfish Lepomis macrochirus: three-dimensional kinematics during propulsion and maneuvering. J Exp Biol. 2005; 208:2753–2763. DOI: 10.1242/jeb.01706 [PubMed: 16000544]
39. Standen EM, Lauder GV. Hydrodynamic function of dorsal and anal fins in brook trout (Salvelinus fontinalis). J Exp Biol. 2007; 210:325–339. DOI: 10.1242/jeb.02661 [PubMed: 17210968]
40. Drucker EG, Lauder GV. A hydrodynamic analysis of fish swimming speed: wake structure and locomotor force in slow and fast labriform swimmers. J Exp Biol. 2000; 203:2379–2393. [PubMed: 10903153]
41. Drucker EG, Lauder GV. Locomotor function of the dorsal fin in rainbow trout: kinematic patterns and hydrodynamic forces. J Exp Biol. 2005; 208:4479–4494. DOI: 10.1242/jeb.01922 [PubMed: 16339868]
42. Quinn DB, Lauder GV, Smits AJ. Scaling the propulsive performance of heaving flexible panels. J Fluid Mech. 2014; 738:250–267. DOI: 10.1017/jfm.2013.597
43. Quinn DB, Lauder GV, Smits AJ. Maximizing the efficiency of a flexible propulsor using experimental optimization. J Fluid Mech. 2015; 767:430–448. DOI: 10.1017/jfm.2015.35
44. Grosberg A, Alford PW, McCain ML, Parker KK. Ensembles of engineered cardiac tissues for physiological and pharmacological study: heart on a chip. Lab on a chip. 2011; 11:4165–4173. DOI: 10.1039/c1lc20557a [PubMed: 22072288]

One Sentence Summary

[A brief summary of the main result of your paper, without excessive jargon and less than 150 characters]

We create a tissue-engineered soft-robotic ray that swims using undulating fin motions, and turns according to externally applied light cues.

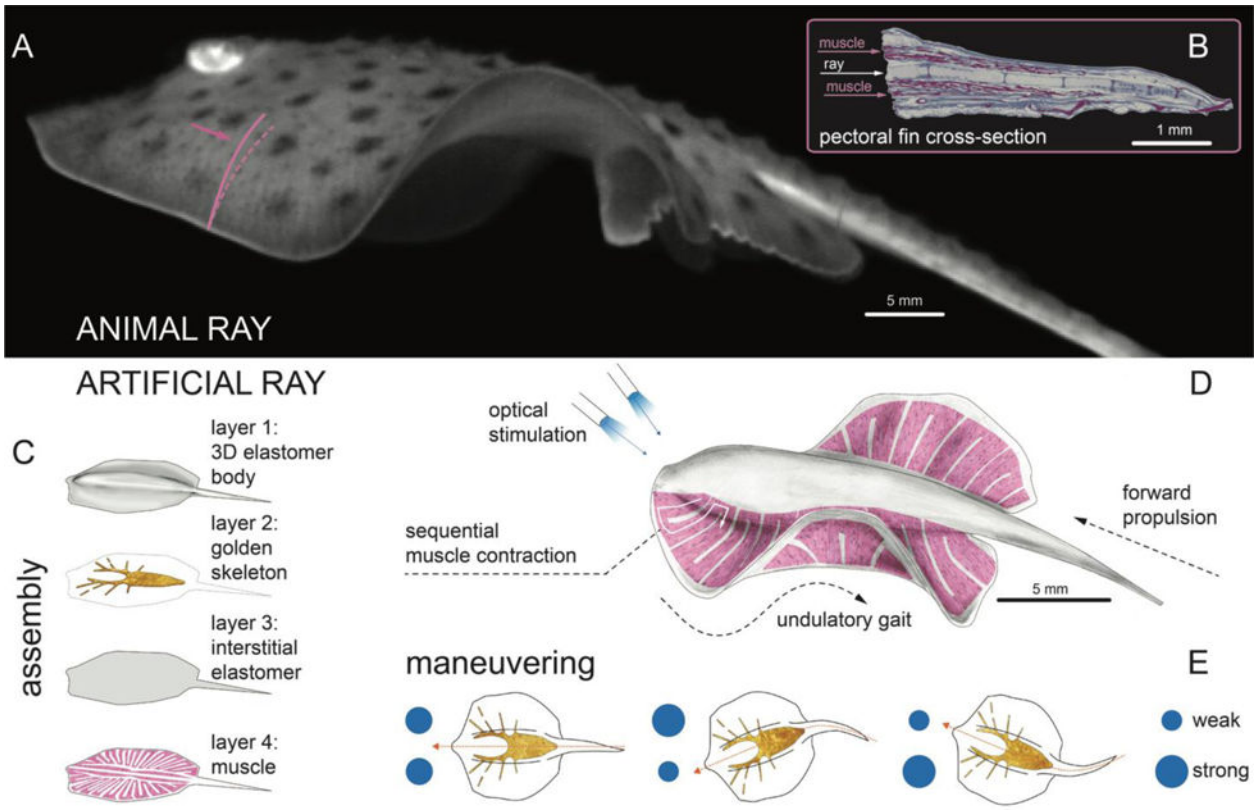

Fig. 1. Bioinspired concept design of the tissue-engineered ray

(A) A live Little skate, *Leucoraja. erinacea*, swimming and (B) its musculoskeletal structure. (C to E) Tissue-engineered ray with four layers of body architecture (C), concept (D), and phototactic control (E). Upon optical stimulation, the tissue-engineered ray induces sequential muscle activation via serpentine patterned muscle tissues, generates undulatory locomotion, and sustains steady forward swimming. It changes directions by generating asymmetric undulating motion between left and right fins, modulated by light pulse frequency.

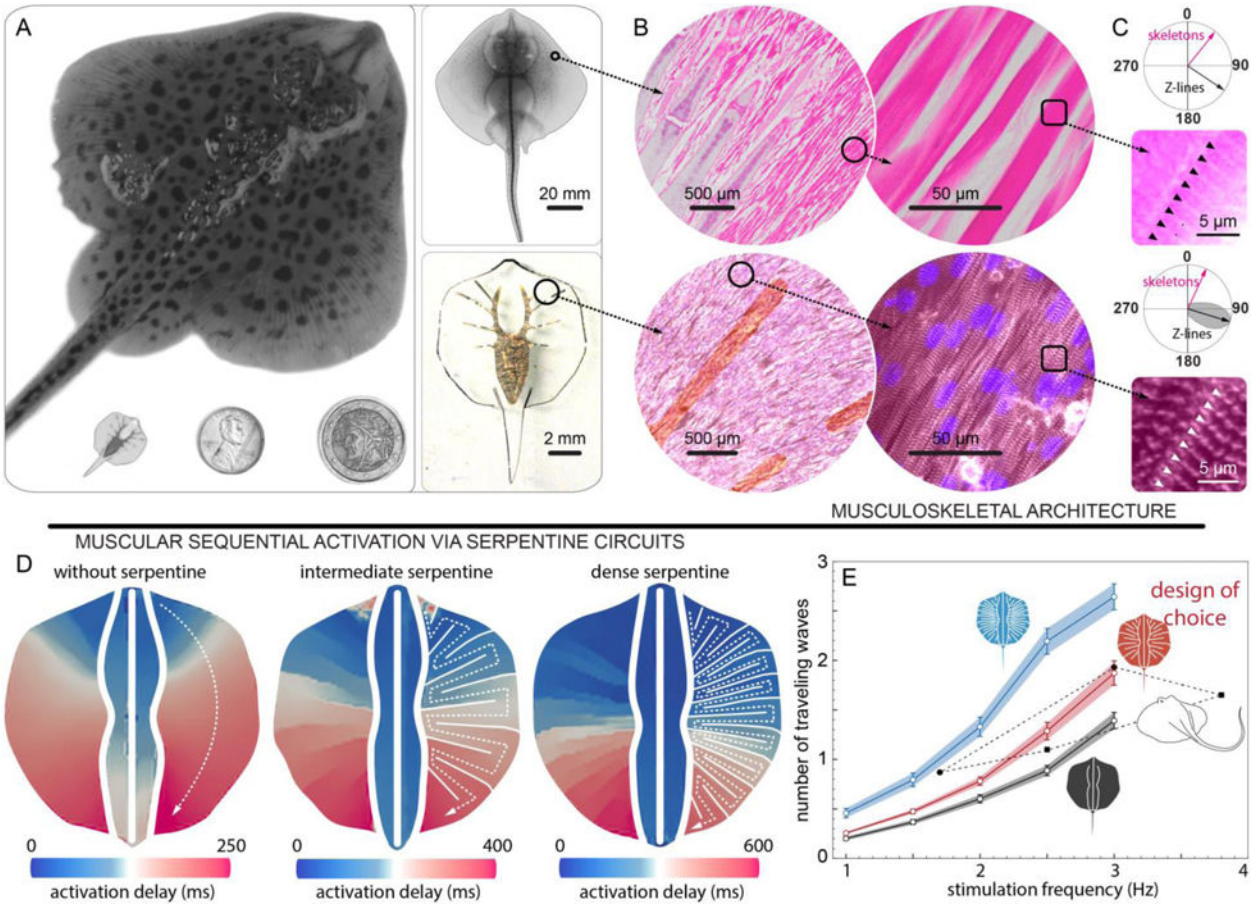

Fig. 2. Engineering solutions

(A) System level design for skate (top) and tissue-engineered ray (bottom left) comparable with one penny and a two Euros coin (bottom middle and right). (B and C) Musculoskeletal (B) meso- and (C) micro-architecture of a skate, *L. erinacea* (top) is replicated in tissue-engineered ray (bottom). Horizontal sections of the skate were stained with hematoxylin and eosin (top) and the engineered tissue was immunostained with a light-sensitive membrane protein, ChR2 (red, bottom left), sarcomeric α-actinin (red, bottom right of B and C), and nuclei (blue, bottom). (C) Orientation of the Z-lines (skate: black arrow and black triangle, top, and tissue-engineered ray: black arrow with gray distribution and white triangle, bottom). In both cases Z-lines are perpendicular to the skeleton rays (pink arrows). (D) Muscle circuits with pre-programmed activation pattern. A point light stimulus directed at the front of the fins with 1.5 Hz frequency triggers the calcium wave that propagates along the predefined serpentine patterns. (E) Operating range of the muscle circuits. The circuit with intermediate serpentine pattern density represents the best tradeoff between contraction time reproducibility (Standard error of the mean, SEM) and overlap with batoids' operating range (*Taeniura. lymma* (20) and *Potamotrygon orbignyi* (22), black symbols). Black, red and blue indicates muscle circuit without serpentine patterns, with intermediate and dense serpentine patterns, respectively. Each colored band indicates SEM of number of traveling waves.

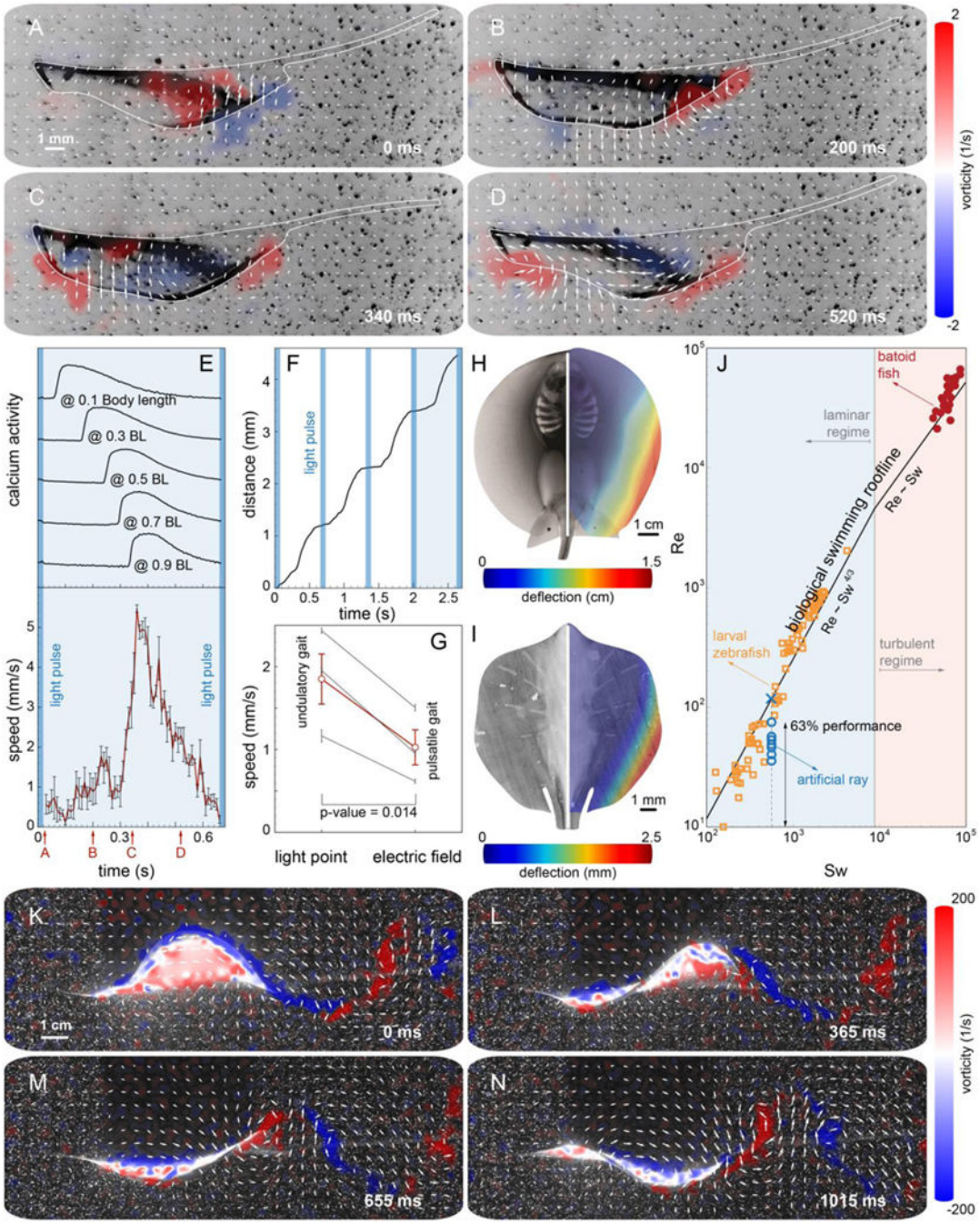

Fig. 3. Kinematics and hydrodynamics

(A to D) PIV flow measurements highlight the production of alternated positive and negative vortices by the tissue-engineered ray. The viscosity associated to the relatively small *Re* is responsible for the dissipation of the vortex street in the wake. (E) Correlation between calcium activity and undulatory locomotion. (F) The moving distance during four strokes. (G) Comparison of swimming speed between the tissue-engineered rays stimulated by point and field stimulations. Undulatory locomotion produced by sequential muscle activation (point: 1.85 mm/s) improved swimming speed significantly compared with pulsatile

propulsion generated by global muscle activation (field: 1.03 mm/s, matched pairs test, p=0.014, n=3 rays). Gray and red lines indicate the speed of individual rays and their average, respectively. (H and I) Out-of-plane fin deflection in both a live stingray, *P. orbignyi* (H) and a tissue-engineered ray (maximum amplitude: 2.54 ± 0.02 mm) (I). (J) Comparison of swimming performance between tissue-engineered rays (n=7 rays) and aquatic swimmers (batoid fish (20) and larval zebrafish (32)) using the scaling analysis (23). (K to M) PIV analysis of live Little skate, *L. erinacea*.

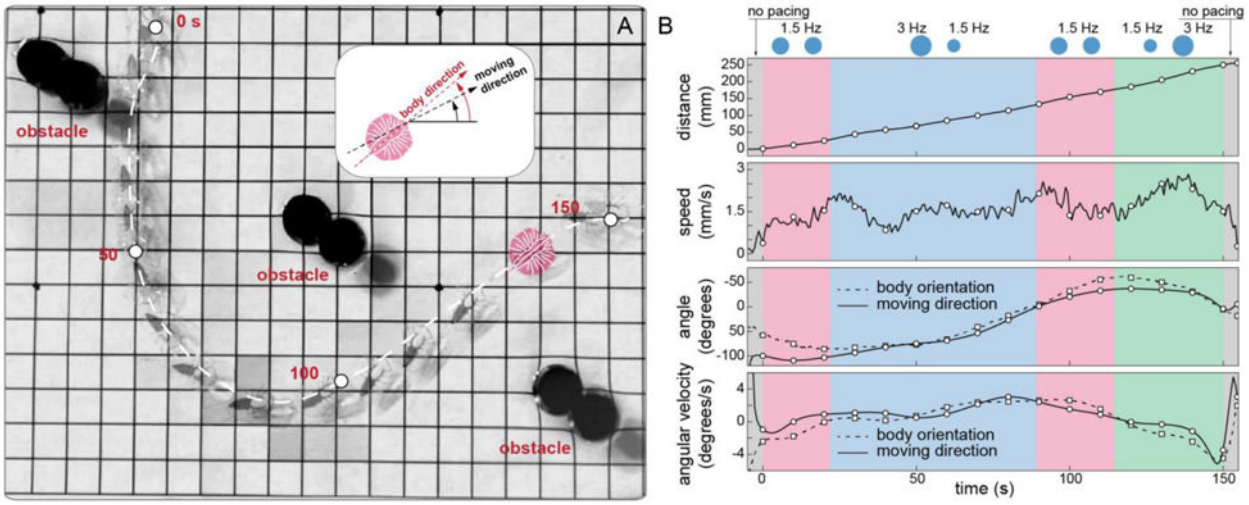

Fig. 4. Phototactic steering of the tissue-engineered ray through an obstacle course

(A) The ray completed a course that required complex coordination and maneuvering. Motion began with a forward protocol (at 0 s) to gain acceleration. A following left turn protocol allowed the ray to overcome forward momentum, making a left turn (at ~50 s). Next, another forward protocol was employed to dissipate counterclockwise angular momentum and regain directionality (at ~100 s). While the ray made its way back to the other side of the obstacles, a final right turn protocol was given to make a right turn, winding the last obstacle. (B) Corresponding kinematic analysis relative to light frequency modulation protocols employed for guidance. Grids, 1 cm.